
Dynamics of the $1^3\Pi_g$ state of K_2 on helium nanodroplets

J. H. Reho,[†] J. P. Higgins and K. K. Lehmann

Department of Chemistry, Princeton University, Princeton, NJ 08544, USA

Received 20th December 2000

First published as an Advance Article on the web 11th June 2001

Fluorescence following optical excitation of the $1^3\Sigma_u^+$ state of K_2 prepared on helium nanodroplets to the predissociative $1^3\Pi_g$ state yields molecular emission from both the (B) $1^1\Pi_u$ and (A) $1^1\Sigma_u^+$ K_2 states as well as atomic emission from the expected $4^2P_{3/2, 1/2} \rightarrow 4^2S_{1/2}$ dissociation channel. A $\sim 12\text{ cm}^{-1}$ red shift is observed in the molecular emission excitation spectrum compared to the atomic emission excitation spectrum. Time-correlated photon counting measurements demonstrate the rise time for both atomic and molecular products to be $< 80\text{ ps}$, independent of vibrational level excited. This lifetime is interpreted as the total depopulation time for the optically excited $1^3\Pi_g$ state, which is dominated by intersystem crossing at low vibrational energy and by predissociation at the highest vibrational level. It is deduced that the timescale for intersystem crossing must be of the order of 10 ps . Symmetry restrictions for the isolated K_2 imply that the intersystem crossing from the $1^3\Pi_g$ state to the (B) $1^1\Pi_u$ and (A) $1^1\Sigma_u^+$ states must be induced by interaction with the helium nanodroplet.

I. Introduction

The helium nanodroplet matrix has been shown to selectively favor the formation of high-spin oligomers of alkali metal atoms against their low-spin (*i.e.*, covalently bound) counterparts. This selectivity has allowed for the measurement of quartet trimer spectra^{1–3} as well as those of homo- and heteronuclear triplet dimers.¹ The vibrationally-resolved, triplet-to-triplet excitations of Na_2 , K_2 and NaK have all been measured using helium nanodroplet isolation spectroscopy.¹ In the course of that work, the dispersed emission following the $1^3\Pi_g \leftarrow 1^3\Sigma_u^+$ excitation of K_2 has been shown to include intensity assigned to the (B) $1^1\Pi_u \rightarrow$ (X) $1^1\Sigma_g^+$ emission of K_2 , thus pointing to the existence of product channels which arise due to a triplet-to-singlet intersystem crossing. In the present paper, this spectrum is reexamined using both wavelength selected excitation spectra and time correlated emission spectroscopy.

II. Experimental

The production of alkali-doped helium nanodroplets will be treated only summarily here, as a more detailed exposition has been given previously.² A beam of He nanodroplets ($\langle N \rangle \sim 10^3\text{--}10^4$) results from a free jet expansion of He gas through a nozzle of $20\text{ }\mu\text{m}$ diameter using a stagnation

[†] Present address: Dynamic Experimentation Division (DX-2), Los Alamos National Laboratory, Los Alamos, NM 87545, USA.

pressure of 2.5 MPa and nozzle temperatures of 16–20 K. This resultant droplet beam is collimated by a 400 μm skimmer and then doped with potassium atoms using the pick-up technique.³ The doped droplets are probed spectroscopically by laser-induced fluorescence (LIF).⁴

The $1^3\Pi_g \leftarrow 1^3\Sigma_u^+$ transition of K_2 was first measured using a continuous-wave Ti : Al_2O_3 laser as described in ref. 1. Due to experimental limitations, this first spectrum extended only up to $14\,050\text{ cm}^{-1}$, although the intensity due to the transition extends further toward higher energy. In this work, the $1^3\Pi_g \leftarrow 1^3\Sigma_u^+$ transition of K_2 was excited using a synchronously-pumped, mode locked Pyridine 2 dye laser (Coherent 700) pumped by the frequency doubled output of a mode-locked Nd : YAG laser (Coherent Antares). The dye laser produced pulses with a linewidth of under 10 cm^{-1} , a 10–12 ps full width at half maximum temporal width, at a 76 MHz repetition frequency. The resulting $1^3\Pi_g \leftarrow 1^3\Sigma_u^+$ K_2 excitation spectrum was collected by monitoring K atomic emission by introducing a band-pass filter⁵ in front of the multialkali cathode photomultiplier tube (PMT) collecting the LIF.

The time-resolved spectra presented here were collected from the same molecular beam apparatus using reversed time-correlated single-photon counting. Again, the procedure and instrumentation (including the substitution of a microchannel plate detector for the PMT) employed have been previously reported⁶ and here we mention only that the dye laser system was fitted with a cavity dumper (Coherent 7220) in order to reduce the repetition rate of the dye laser output to 3.8 MHz. The count rates encountered in these investigations (typically 1000–5000 counts per second) were insufficient to bias the fluorescence detection by pile-up error, thus ensuring a faithful sampling of the time-resolved emission. Our reversed time-correlated single-photon counting instrument has a nominal resolvability of 20 ps, defined as one-tenth of the full width at half-maximum of the instrument response function.⁷

III. The $1^3\Pi_g \leftarrow 1^3\Sigma_u^+$ transition of K_2

The $1^3\Pi_g \leftarrow 1^3\Sigma_u^+$ spectrum of K_2 residing on a helium nanodroplet surface reveals a broad absorption centered near $13\,950\text{ cm}^{-1}$, which represents a blue shift of about 900 cm^{-1} from the position of the $4^2P_{3/2, 1/2} \leftarrow 4^2S_{1/2}$ K atomic transitions. The original spectrum, measured by the CW Ti : Al_2O_3 laser, and the present spectrum, taken with the mode-locked dye laser, are compared in Fig. 1. It is seen that the scanned range of the dye laser includes the entire region of $1^3\Pi_g \leftarrow 1^3\Sigma_u^+$ K_2 intensity. In neither spectrum is clear vibrational resolution of the $1^3\Pi_g$ achieved, although the laser resolution in both cases should have been sufficient to do so, as will be shown below in discussing the K_2 $1^3\Pi_g$ potential energy surface. Thus the broadness of the spectrum is attributed to effects of the helium matrix on the K_2 dimer. The low-frequency ends of the spectra given in Fig. 1 show slight differences. The spectrum collected using the Ti : Al_2O_3 laser, in which the total fluorescence is collected, shows a small red shoulder and a wider blue wing, which are both absent in the dye laser spectrum. In the dye laser spectrum only the K $4^2P \rightarrow 4^2S$ atomic emission, the expected product from the predissociative $1^3\Pi_g$ state of K_2 , was collected.⁵ The cause of these differences will be discussed below.

Upon dispersing the emission produced by $1^3\Pi_g \leftarrow 1^3\Sigma_u^+$ excitation of K_2 , intensity assigned to the (B) $1^1\Pi_u \rightarrow$ (X) $1^1\Sigma_g^+$ transition was observed. This can be considered surprising in the light of the following facts: (1) intramolecular interactions cannot mix the $1^3\Pi_g$ and (B) $1^1\Pi_u$ states of K_2 ; (2) there is a substantial barrier to formation of the (B) $1^1\Pi_u$ state from the K(4^2S) + K(4^2P) expected to be produced by the adiabatic dissociation of the $1^3\Pi_g$ state. The $1^3\Pi_g \leftarrow 1^3\Sigma_u^+$ excitation spectrum of K_2 was remeasured using the dye laser but employing selective collection of the (B) $1^1\Pi_u \rightarrow$ (X) $1^1\Sigma_g^+$ and then the (A) $1^1\Sigma_u^+ \rightarrow$ (X) $1^1\Sigma_g^+$ K_2 molecular emissions⁸ (Fig. 2). The band pass filters used in these measurements blocked the $4^2P \rightarrow 4^2S$ emission from K atoms. It is seen that two main differences exist between the excitation spectra measured collecting K atomic fluorescence and the spectra collecting either of the molecular products. First, the excitation spectra collected by selecting the molecular products are red-shifted approximately 12 cm^{-1} from the spectrum in which K atomic emission is collected. Second, the blue shoulder present in the spectrum in which the K atomic P \rightarrow S emission is collected is significantly reduced in intensity in the case of molecular emission product collection. The significance of these observations will be discussed below. The two molecular detected excitation spectra appear identical except for the much lower signal to noise realized when detecting (A) $1^1\Sigma_u^+$ rather than (B) $1^1\Pi_u$ emission.

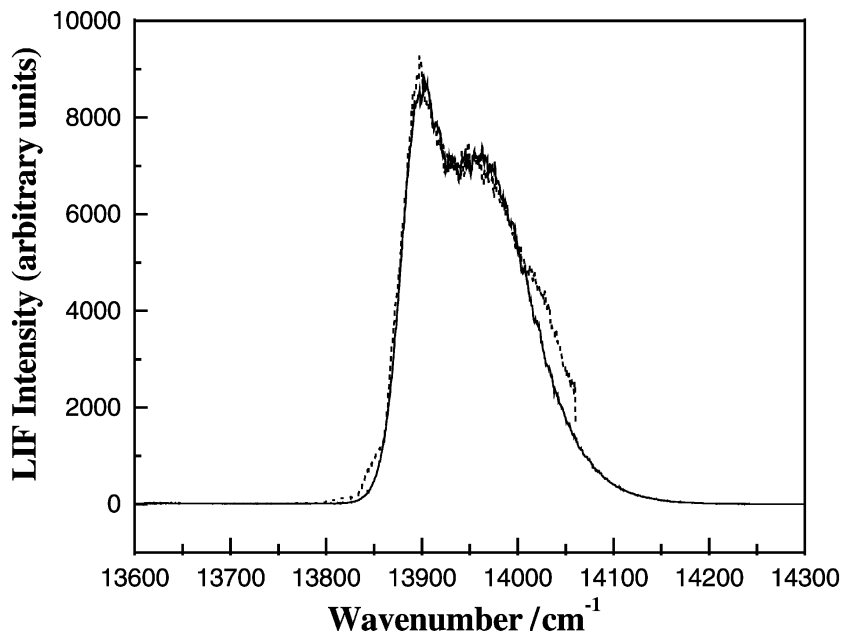


Fig. 1 The $1^3\Pi_g \leftarrow 1^3\Sigma_u^+$ excitation spectrum of K_2 on helium nanodroplets. The dotted curve corresponds to the spectrum collected using a CW $Ti : Al_2O_3$ laser in which the total fluorescence was collected and the solid curve to the spectrum collected using a mode locked dye laser in which only the K atomic fluorescence was collected. The intensities of the spectra are normalized for the sake of comparison. Note the absence of the red shoulder in the case of K atomic fluorescence collection.

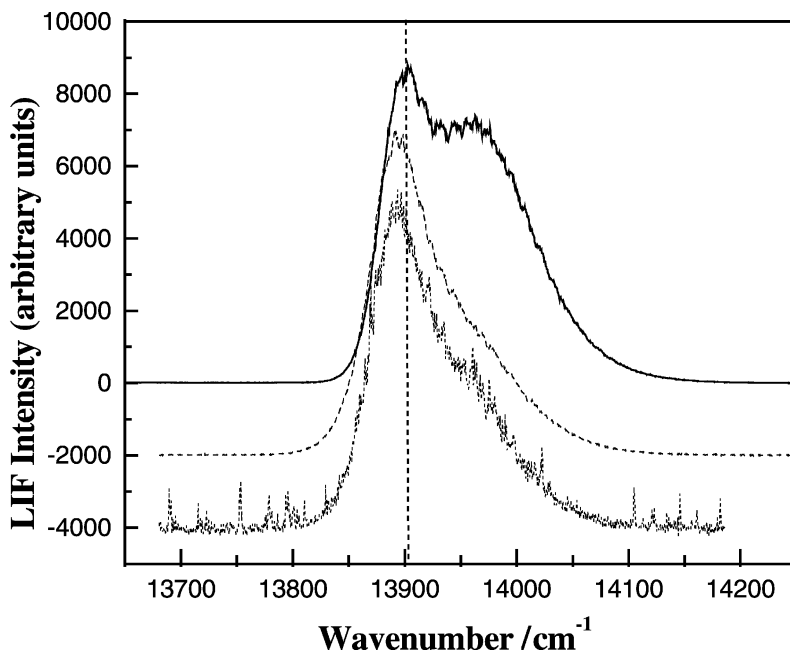


Fig. 2 The $1^3\Pi_g \leftarrow 1^3\Sigma_u^+$ excitation of K_2 on helium nanodroplets employing selective collection. Solid spectrum: collection of K $4^2P \rightarrow 4^2S$ fluorescence. Dashed spectrum: collection of K_2 (B) $1^1\Pi_u \rightarrow (X)1^1\Sigma_g^+$ fluorescence. Dotted spectrum: collection of K_2 (A) $1^1\Sigma_u^+ \rightarrow (X)1^1\Sigma_g^+$ fluorescence. The position of the maximum of the spectrum obtained by collecting K $4^2P \rightarrow 4^2S$ fluorescence is given by the vertical dotted line. The dashed spectrum has been vertically shifted by -2000 and the dotted spectrum by -4000 for clarity.

Measuring the actual branching ratios of the three spectra given in Fig. 2 is complicated by the fact that the quantum efficiency of the microchannel plate detector drops off rapidly for wavelengths longer than 700 nm, and thus does not detect the (A) $1^1\Sigma_u^+ \rightarrow$ (X) $1^1\Sigma_g^+$ fluorescence efficiently. However, using the red-enhanced PMT, a rough comparison of the total fluorescence excitation spectra, with that in which only $K\ 4^2P \rightarrow 4^2S$ atomic fluorescence was collected reveals that the largest fraction ($>70\%$) of the total fluorescence is due to atomic emission, except at the red edge of the spectrum. Thus the rate of predissociation dominates over that of intersystem crossing. This result stands in contrast to the intersystem crossing of Na_3 and K_3 measured previously in our laboratory,^{1,2} in which a large majority of fluorescence was found to arise from the intersystem crossing product channels. In those cases, however, the intersystem crossing needs only to compete with radiative relaxation.

IV. Time-resolved spectra of the $1^3\Pi_g$ K_2 emission channels

The production of singlet dimer fluorescence upon $1^3\Pi_g \leftarrow 1^3\Sigma_u^+$ excitation of K_2 has been time resolved using the reversed time-correlated single-photon counting technique. Both the fluorescence onset times and the respective lifetimes of the atomic and molecular products have been measured. Fig. 3 shows the temporally-dispersed (B) $1^1\Pi_u \rightarrow$ (X) $1^1\Sigma_g^+$ K_2 emission collected from excitation at differing wavelengths (shown in the inset of Fig. 3). Fig. 4 shows the same time-resolved emission, but highlights the fluorescence onset in order to show the extent of reproducibility irrespective of excitation frequency. Such time-resolved emissions were found to be identical upon excitation at various frequencies spanning the area of the $1^3\Pi_g \leftarrow 1^3\Sigma_u^+$ transition, including frequencies corresponding to the red shoulder of the excitation spectrum ($13\ 855\text{ cm}^{-1}$).

Fits to our spectra were conducted using a single-exponential rise, single-exponential fall model which has been described previously,⁹ and yielded satisfactory agreement with the data, based upon a standard χ^2 analysis. All fits to the time-resolved (B) $1^1\Pi_u \rightarrow$ (X) $1^1\Sigma_g^+$ K_2 emission yielded fluorescence rise times of 60 ± 20 ps and fall times of 11.5 ± 0.4 ns. Time resolution of the (A) $1^1\Sigma_u^+ \rightarrow$ (X) $1^1\Sigma_g^+$ molecular K_2 fluorescence was impeded by the poor quantum efficiency of the microchannel plate detector in that frequency region. The results of our time-resolved measurements are given in Table 1. A representative fit to the time-resolved data obtained by exciting the $1^3\Pi_g \leftarrow 1^3\Sigma_u^+$ transition at $13\ 855\text{ cm}^{-1}$ is displayed in Fig. 5 along with the instrument response function and the residual of the fit. From Table 1 it is seen that the measured lifetime of

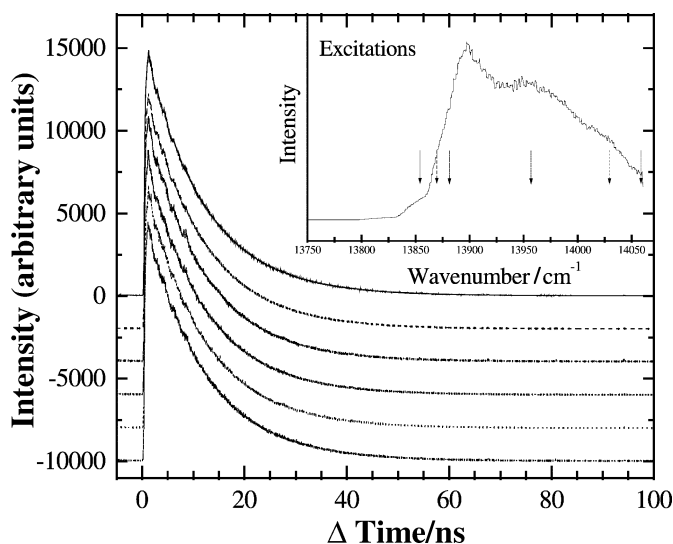


Fig. 3 Time-resolved (B) $1^1\Pi_u \rightarrow$ (X) $1^1\Sigma_g^+$ fluorescence of K_2 collected upon excitations of the $1^3\Pi_g \leftarrow 1^3\Sigma_u^+$ transition of K_2 on helium droplets. The excitation frequencies are shown in the inset. Each successive spectrum has been vertically offset by -2000 for clarity.

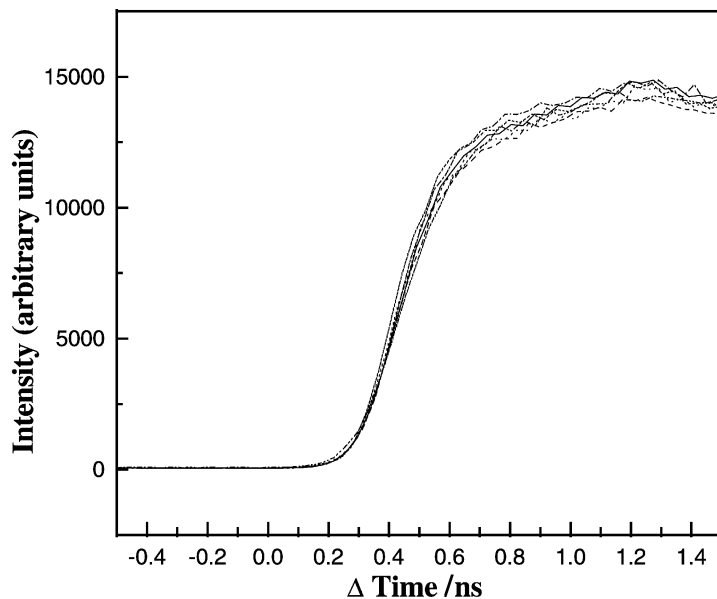


Fig. 4 The fluorescence onsets of the $(B)1^1\Pi_u \rightarrow (X)1^1\Sigma_g^+$ K_2 emission upon $1^3\Pi_g \leftarrow 1^3\Sigma_u^+$ excitation at the frequencies given in Fig. 3. Note the agreement of the rising edges.

K atom (27.0 ± 0.4 ns) agrees well with the gas phase lifetime values of 26.34 ns (for $4^2P_{3/2}$) and 26.69 ns (for $4^2P_{1/2}$) measured by photoassociative spectroscopy.¹⁰ Similar agreement is found between the measured lifetimes of the K_2 $(B)1^1\Pi_u$ state (11.5 ± 0.4 ns) and the value (11 ± 1.1 ns) reported in the literature.¹¹ We note that the good fit of the experimental decay to a single-exponential fall time that agrees in all cases with the respective gas phase values indicates that both the K $4^2P \rightarrow 4^2S$ and the K_2 $(B)1^1\Pi_u \rightarrow (X)1^1\Sigma_g^+$ emission occur in the gas phase, *i.e.*, the species completely desorb from the helium droplet on a much earlier timescale than that of their spontaneous emission.

The finite onset time of fluorescence for the molecular product channel reflects the lifetime of the K_2 $1^3\Pi_g$ state, which arises from both predissociation and from intersystem crossing time from the triplet to the singlet manifold. It is found from Table 1 that the onset of fluorescence from the $(B)1^1\Pi_u$ state of K_2 occurs with a rise time of 60 ± 20 ps, while the rise time of the atomic emission is fit to 50 ± 20 ps. A magnified view of the fit to the data shown in Fig. 5 is displayed in Fig. 6, highlighting the rise time of the fluorescence. Two fits are shown: the first with

Table 1 Gas phase fluorescence onset times (rise times) and lifetimes (fall times) of K $4^2P \rightarrow 4^2S$ and $K_2(B)1^1\Pi_u \rightarrow (X)1^1\Sigma_g^+$ upon $1^3\Pi_g \leftarrow 1^3\Sigma_u^+$ excitation of K_2 on the surface of helium nanodroplets

Excitation /cm ⁻¹	Rise time	Lifetime	Rise time	Lifetime
	/ps (± 20 ps)	/ns (± 0.4 ns)	/ps (± 20 ps)	/ns (± 0.4 ns)
	K_2 $(B)1^1\Pi_u \rightarrow (X)1^1\Sigma_g^+$		K $4^2P \rightarrow 4^2S$	
13 855	67	11.51	50	27.1
13 870	65	11.45	43	26.8
13 882	53	11.48	47	27.0
13 956	59	11.45	51	27.1
14 031	67	11.46	55	27.2
14 058	71	11.49	52	27.0
Mean	63.7	11.47	49.7	27.03
Std. deviation	5.96	0.02	3.82	0.12

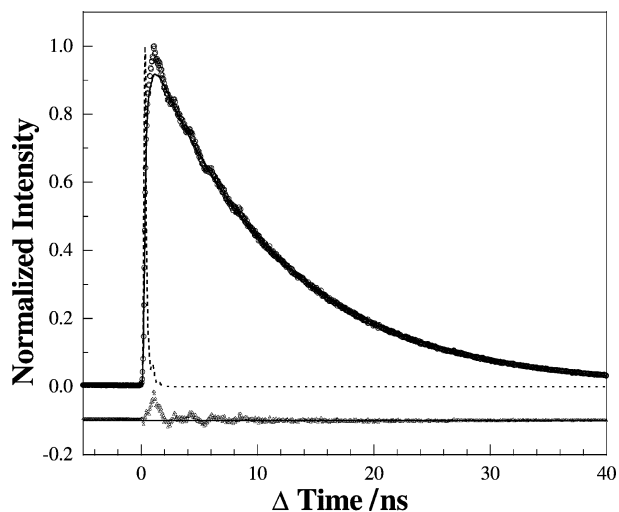


Fig. 5 Time-resolved (B) $1^1\Pi_u \rightarrow (X)1^1\Sigma_g^+$ fluorescence of K_2 collected upon excitation at 13855 cm^{-1} of the $1^3\Pi_g \leftarrow 1^3\Sigma_u^+$ transition of K_2 (\circ). The fit to the data using a single-exponential rise and single-exponential fall is given by the solid line. A rise time of 67 ps and a fall time of 11.51 ns is used in the fit. The instrument response function is given by the dashed line. The residual of the fit is shown as (Δ). A factor of -0.1 is added to the residual of the fit for clarity.

a rise time of 67 ps which minimizes the χ^2 of the fit, and the other with a 20 ps rise time. It is clear that the fit employing a rise 67 ps produces a smaller residual. Both rise times may in fact be instrument-limited, as there is only a small increase in χ^2 when an instrument-limited rise is employed in our model for the molecular emissions. As a result, we can conservatively conclude

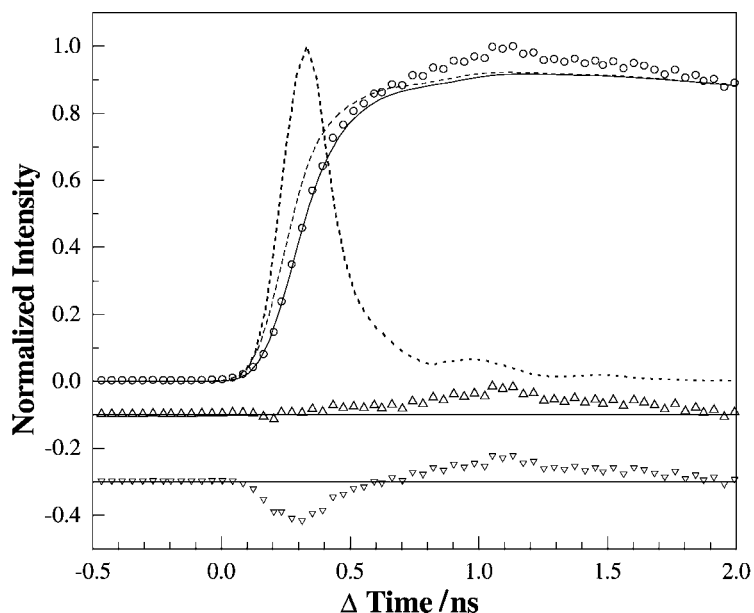


Fig. 6 Magnified view of the fluorescence onset of the (B) $1^1\Pi_u \rightarrow (X)1^1\Sigma_g^+$ K_2 emission upon $1^3\Pi_g \leftarrow 1^3\Sigma_u^+$ excitation at 13855 cm^{-1} (\circ). The fit employing a rise time of 67 ps is shown by the solid line with the corresponding residual shown by (Δ) (a factor of -0.1 is added for clarity). The fit employing a rise time of 20 ps is shown by the dashed line with the corresponding residual shown by (∇) (a factor of -0.3 is added for clarity). The instrument response function is given by the dotted line.

that the upper bound for the depletion time of the K_2 $1^3\Pi_g$ state is 80 ps, independent of the vibrational level to which this state is excited.

V. The $1^3\Pi_g$ potential energy surface of K_2

Ab initio calculations of the $1^3\Pi_g$ potential energy surface of K_2 can be found in the literature.^{12,13} The surfaces of both Jeung and Ross¹² and Magnier¹³ include the presence of a well at short internuclear range in addition to the expected long range R^{-3} repulsion. These potential energy surfaces, as well as the $1^3\Sigma_u^+$ RKR (Rydberg–Klein–Rees) surface of Li and coworkers,¹⁴ are shown in Fig 7. It is seen that while both $1^3\Pi_g$ surfaces agree in the internuclear distance of the well, the well depth predicted by Jeung and Ross is more than twice that of Magnier. Also shown in the figure, and given in Table 2, are the positions and Franck–Condon factors for absorption from the ground vibrational level of the $1^3\Sigma_u^+$ state. It is evident that the predicted absorption spectra are very different. The lifetimes of the four quasi-bound levels predicted from the Magnier surface (using the BCONT program of LeRoy¹⁵) as well as the two highest levels of the Jeung and Ross potential are also given in Table 2.

Fig. 8 contains a comparison of the experimental $1^3\Pi_g \leftarrow 1^3\Sigma_u^+$ K_2 excitation spectrum with those predicted by the two surfaces. It is evident that the Jeung and Ross surface predicts an absorption spectrum in poor agreement with experiment, predicting almost all the absorption intensity to fall to the red of the observed spectrum. Excellent agreement is found between the experimental spectrum below 13920 cm^{-1} and the spectrum predicted from the $1^3\Pi_g$ surface of Magnier¹³ in combination with the $1^3\Sigma_u^+$ RKR surface.¹⁴ In particular, the extreme red wing of the spectrum matches that predicted as arising from the $v' = 0$ and $1 \leftarrow v'' = 0$ transitions. This

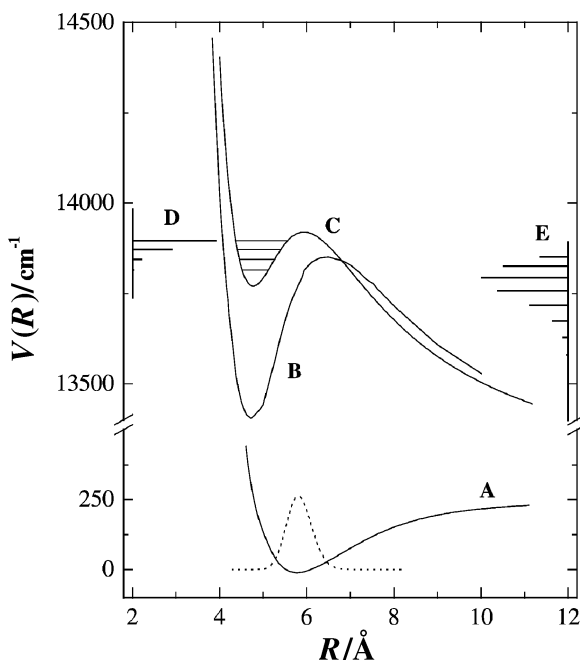


Fig. 7 The potential energy surfaces of triplet K_2 . A: The RKR $1^3\Sigma_u^+$ surface of Li and coworkers,¹⁴ including the wavefunction for $v'' = 0$ (dotted curve). The lower state (A) has been shifted by $+243\text{ cm}^{-1}$ along with the excited state to make the $v'' = 0$ level coincide with the zero of the energy. B: The K_2 $1^3\Pi_g$ surface as calculated by Jeung and Ross.¹² C: The K_2 $1^3\Pi_g$ surface as calculated by Magnier¹³ showing the excited state levels $v' = 0-4$. D: The calculated center frequencies and intensities of the bound–bound transitions of the $1^3\Pi_g \leftarrow 1^3\Sigma_u^+$ transition of K_2 using the $1^3\Pi_g$ potential of Magnier.¹³ E: The calculated center frequencies and intensities of the bound–bound transitions of the $1^3\Pi_g \leftarrow 1^3\Sigma_u^+$ transition of K_2 using the $1^3\Pi_g$ potential of Jeung and Ross.¹²

Table 2 Calculated positions, relative Frank–Condon factors (FCF), and lifetimes of the quasi-bound $1^3\Pi_g$ vibrational levels of K_2 based upon the excited state potential curves of Magnier¹³ and Jeung and Ross.¹² The $T(v)$ values are referenced to the $v'' = 0$ level of the RKR $1^3\Sigma_u^+$ surface of Li and coworkers.¹⁴ The relative Frank–Condon factors have been normalized to the most intense transition ($v' = 3$) calculated using the Magnier potential. The lifetimes of the $v' = 0$ –8 levels calculated using the potential of Jeung and Ross.¹² are all greater than 1 μ s, a time-scale greater than the radiative lifetime

$1^3\Pi_g$ Vibrational level (v')	$T(v)/\text{cm}^{-1}$	Relative FCF	Lifetime/ps
Magnier			
0	13 815	6.82×10^{-3}	210
1	13 844	8.37×10^{-2}	53
2	13 872	0.337	21
3	13 896	1.00	2.75
Jeung and Ross			
0	13 430	5.51×10^{-5}	N/A
1	13 477	5.85×10^{-4}	N/A
2	13 530	3.40×10^{-3}	N/A
3	13 580	1.79×10^{-2}	N/A
4	13 628	6.12×10^{-2}	N/A
5	13 674	0.179	N/A
6	13 717	0.440	N/A
7	13 757	0.798	N/A
8	13 793	0.983	N/A
9	13 825	0.731	785
10	13 851	0.320	7.79

indicates that the Magnier $1^3\Pi_g$ surface possesses very nearly the correct well depth and harmonic frequency. The observed spectrum does indicate a broadening beyond the lifetime broadening of the quasibound levels, which are indicated in Fig. 8. Further, the experimental spectrum has a second absorption peak, centered around $13\,960\text{ cm}^{-1}$, which is not reproduced by the Magnier surface, even when transitions directly into the continuum (the weak peak predicted near $13\,920\text{ cm}^{-1}$) are included in the simulation. We assign this second peak as arising from the presence of a phonon side band built upon the pure electronic excitation. The spacing and width of this peak are similar to that observed in other electronic transitions of triplet state alkali dimers on the surface of helium nanodroplets.¹

VI. Discussion

The selectively-collected excitation spectra of K_2 upon $1^3\Pi_g \leftarrow 1^3\Sigma_u^+$ excitation differ in onset for the collection of molecular and atomic products. In particular, the transitions to the $v' = 0$ and 1 levels do not appear to lead to significant $K(4^2P)$ production. As shown in Table 2, these levels of the $1^3\Pi_g$ state are predicted to have long predissociation lifetimes, 210 and 53 ps respectively. This suggests that the $1^3\Pi_g$ to $(B)1^1\Pi_u$ relaxation rate, which by symmetry must be induced by interaction with the helium, must lead to a lifetime much shorter than this, and thus little branching ratio to the predissociation products. In contrast, the excitation to the $v' = 2$ and 3 levels leads to efficient production of $K(4^2P)$. These levels are predicted by the Magnier potential to have predissociation lifetimes of 21 and 2.8 ps respectively. Thus, the $\sim 12\text{ cm}^{-1}$ red shift observed when collecting the molecular products likely reflects the changing competition between predissociation and intersystem crossing with vibrational energy in the $1^3\Pi_g$ state. While it is not possible to be quantitative because of the uncertainty of the predissociation rates, one can use two facts to give an estimate for the intersystem crossing rate. One is that even for the lowest levels of the

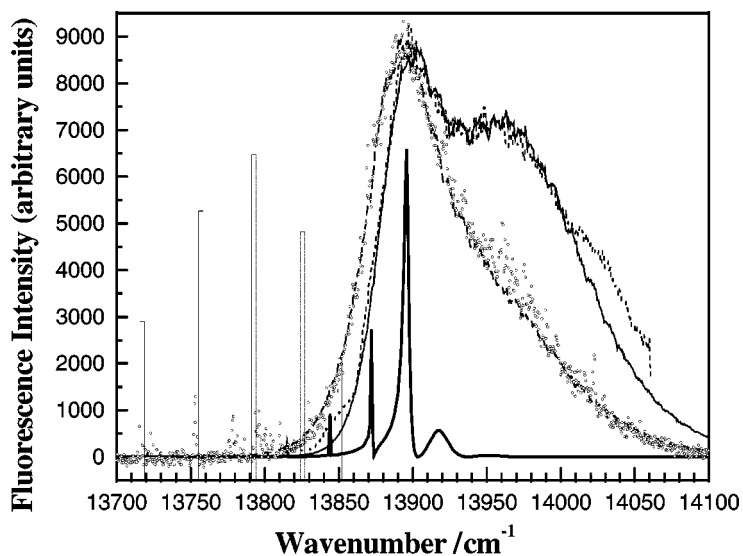


Fig. 8 Comparison of the calculated $1^3\Pi_g \leftarrow 1^3\Sigma_u^+$ spectra of K_2 with the experimental spectra of the same transition measured on helium nanodroplets. Total fluorescence collection using a CW Ti:Al₂O₃ laser (dotted line) and by a quasi-cw dye laser (thin solid line). The excitation spectra obtained by fluorescence collection of the molecular products are shown by the dashed line for (B) $1^1\Pi_u \rightarrow (X)1^1\Sigma_g^+$ emission and by the open circles for K_2 (A) $1^1\Sigma_u^+ \rightarrow (X)1^1\Sigma_g^+$ emission. The calculated spectrum obtained using the Magnier potential¹³ is shown by the thick solid line while the open bars display the calculated transitions using the potential of Jeung and Ross.¹²

$1^3\Pi_g$ state, the observed lifetime is less than 80 ps. Thus the intersystem crossing rate must occur on a time less than this. Second, for the highest vibrational level of the $1^3\Pi_g$ state, which should have a predissociation lifetime of ~ 1 ps, the predissociation dominates over intersystem crossing. Thus, we can conclude that the intersystem crossing likely occurs on a timescale of the order of 10 ps, remarkably fast when one considers that it must be induced by interaction with the helium since no intramolecular vibronic interaction will mix g and u symmetry states.

One remaining experimental observation remains to be rationalized. This is the fact that the blue peak, which we assign as a ‘phonon wing’, falls off much faster when detecting the molecular products. One possible interpretation is that the Magnier potential underestimates the height of the potential maximum, and that several more vibrational levels are quasibound behind the barrier. This, we believe, is unlikely for two reasons. First, the long range repulsion of the $1^3\Pi_g$ state arises from the resonant dipole–dipole interaction between the two K atoms, and thus the $1^3\Pi_g$ is unlikely to rise at long range faster than predicted. Second, if the barrier was substantially higher, then the predissociation lifetimes of the $v' = 2$ and 3 levels would be much longer than predicted by the Magnier potential. In that case, it seems hard to reconcile the observation of fast decay and the efficient production of the dissociation products when these quasibound levels are populated. An alternative explanation starts with the recognition that the peak of this assigned phonon wing involves depositing ~ 70 cm⁻¹ in vibrational excitation in the helium droplet. This could lead to rapid evaporation of the K_2 from the droplet, which would be expected to shut off the intersystem crossing as this requires interaction with the helium. Thus, the relative yield of the molecular products would be expected to fall with increasing energy deposited into the helium droplet phonon and ripplon modes, which is consistent with the observations.

Acknowledgements

We gratefully acknowledge helpful discussions with and the support of G. Scoles. This work was carried out under Grant No. F49620-98-1-0045 of the AFOSR HEDM program.

References

- 1 J. Higgins, C. Callegari, J. Reho, F. Stienkemeier, W. E. Ernst, K. K. Lehmann and G. Scoles, *J. Phys. Chem. A*, 1996, **102**, 4951.
- 2 F. Stienkemeier, J. Higgins, C. Callegari, S. I. Kanorsky and G. Scoles, *Z. Phys. D*, 1998, **38**, 253.
- 3 T. E. Gough, M. Mengel, P. A. Rowntree and G. Scoles, *J. Chem. Phys.*, 1985, **83**, 4958.
- 4 U. Hefter and K. Bergmann, in *Atomic and Molecular Beam Methods*, ed. G. Scoles, Oxford University Press, New York, 1988, vol. 1, ch. 9, pp. 241–242.
- 5 The selective collection of the emission coming from the $4^2P_{3/2, 1/2}$ states of K atoms was done using an Andover 766FS10-50 bandpass filter.
- 6 J. Reho, J. Higgins, K. K. Lehmann and G. Scoles, *J. Chem. Phys.*, 2000, **113**, 9694.
- 7 D. V. O'Connor and D. Phillips, *Time-correlated Single Photon Counting*, Academic Press, San Diego, 1984.
- 8 Selective collection was accomplished using Andover bandpass filters 650FS80-50 (for collection of K_2 B \rightarrow X emission) and Andover 850FS40-50 (for collection of K_2 A \rightarrow X emission).
- 9 J. Reho, C. Callegari, J. Higgins, W. E. Ernst, K. K. Lehmann and G. Scoles, *Faraday Discuss.*, 1997, **108**, 161.
- 10 H. Wang, J. Li, X. T. Wang, C. J. Williams, P. L. Gould and W. C. Stwalley, *Phys. Rev. A*, 1997, **55**, R1569.
- 11 A. A. Radzig and B. M. Smirnov, *Reference Data on Atoms, Molecules and Ions*, Springer-Verlag, Berlin, 1985, p. 385.
- 12 G.-H. Jeung and A. J. Ross, *J. Phys. B*, 1988, **21**, 1473.
- 13 S. Magnier, Doctoral Dissertation, Université de Paris-Sud, Centre d'Orsay, 1993.
- 14 L. Li, A. M. Lyyra, W. T. Luh and W. C. Stwalley, *J. Chem. Phys.*, 1984, **93**, 1215.
- 15 R. J. LeRoy, *Comput. Phys. Commun.*, 1989, **52**, 383.